# Relaxation and polarization effects in valence photodetachment of the negative chloride ion

M. Kutzner, J. A. Robertson, and P. Pelley
*Department of Physics, Andrews University, Berrien Springs, Michigan 49104*
(Received 12 June 2000; revised manuscript received 4 August 2000; published 14 November 2000)

The photodetachment cross section, radiative attachment cross section, branching ratio, and angular-distribution asymmetry parameter have been calculated for $Cl^-$ in the relativistic random-phase approximation (RRPA) and modifications of the RRPA which allow for the inclusion of relaxation and polarization effects. Photodetachment cross sections are compared with experiment to assess the effectiveness of the various approximations.

PACS number(s): 34.80.Gs

Aside from the need for accurate opacity and radiative attachment data for negative ions in astrophysics, atmospheric physics, and plasma chemistry [1], the study of photodetachment of such systems provides important insight into many-body effects in the absence of a long-range Coulomb attraction by the nucleus. Such effects are especially important near threshold where a slow-moving photoelectron has ample time to interact with the spectator electrons of the neutral atom left behind. In particular, the interaction representing the long-range polarization potential should be considered for negative ions because the self-consistent Hartree-Fock field acting on the photoelectrons is of short range.

The photodetachment cross section of the negative chloride ion was measured by Mandl [2] and others [3] over two decades ago. Theoretical calculations of this cross section include the early single-particle model calculations of Robinson and Geltman [4], many-body perturbation theory (MBPT) calculations of Qian and Kelly [5] and Ishihara and Foster [6], the method of Stieltjes calculations of Rescigno *et al.* [7], and the relativistic random-phase approximation (RRPA) calculations of Radojević *et al.* [8]. Kutzner *et al.* [9] used RRPA photodetachment cross sections to determine frequency-dependent polarizabilities of $Cl^-$ and other halide anions.

The present study investigates the effects of core relaxation and polarization in the photodetachment process. We have employed the RRPA [10], the RRPA modified to include relaxation effects (RRPAR) [11], and a new modification of the RRPA that approximately includes both core relaxation and polarization (RRPARP).

Various techniques have been used to account for core polarization in photoionization. Kutzner *et al.* [12] included relaxation and polarization effects in a study of the photoionization of $4d$ electrons of atomic barium using the appropriate second-order diagrams in many-body perturbation theory. The classes of MBPT diagrams representing the random-phase approximation (RPA) and various relaxation and polarization effects are shown in Fig. 1. The relaxation and polarization diagrams have opposite signs since rules for writing MBPT diagrams prescribe that the overall sign of a diagram alternates with the total number of hole lines. The relaxation and polarization diagrams thus tend to cancel one another at higher energy. A more physical interpretation of this cancellation is that including polarization allows the photoelectron to partially ''fill'' the vacancy created by the inclusion of relaxation effects.

Alternatively, theoreticians have approximated effects of core polarization using various modifications to the photoelectron potential. The eigenchannel *R*-matrix approach used by Greene and Aymar [13] for alkaline earth systems and Robicheaux and Greene [14] for calculations of neutral halogens uses polarization potentials with the form [15]

$$V_{\mathrm{pol}}(r) = -\frac{\alpha_d}{2r^4} W_c(r), \tag{1}$$

where $\alpha_d$ is the dipole polarizability of the core and $W_c(r)$ is a cutoff function to prevent the potential from becoming unmanageable at the origin. Forms of the cutoff function vary slightly from [13]

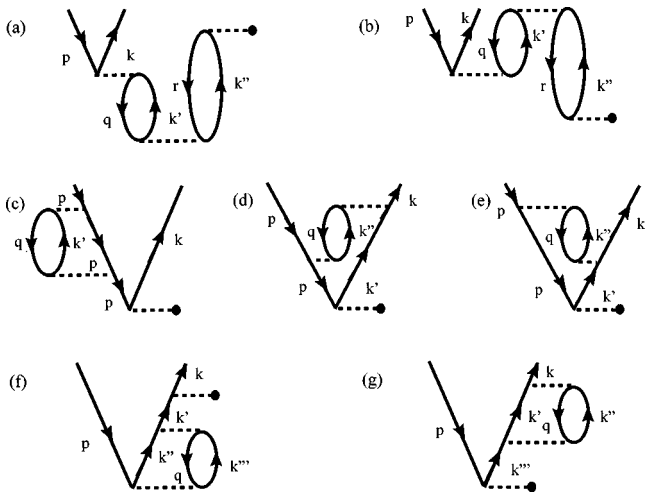


FIG. 1. Second-order diagrams in many-body perturbation theory contributing to the transition $p \rightarrow k$. Time proceeds from bottom to top; particles (holes) are represented by lines with arrows directed upward (downward); dashed lines ending with a solid dot indicate a dipole matrix element; other dashed lines represent Coulomb interactions. (a),(b) Diagrams included to all orders in the RRPA. (c) Energy correction diagram on the hole line. (d),(e) Relaxation diagrams. (f) Polarization in the ground state. This diagram contributes to the ''Brueckner orbital.'' (g) Polarization diagram for the final-state orbital or inelastic scattering of photoelectron. All diagrams have exchange counterparts.

 

$$W_c(r)=\{1-\exp[-(r/r_c)^3]\}^6 \tag{2}$$

to [14]

$$W_c(r)=1-\exp[-(r/r_c)^m] \tag{3}$$

depending on the particular species under consideration. In Eqs. (2) and (3), $r_c$ is a cutoff radius determined, along with $\alpha_d$, semiempirically by optimizing the fitted agreement between the calculated energy levels and the experimental levels of the ion [15]. This approach cannot be applied to a negative ion having no bound-excited states.

The technique used in this study was proposed by Amusia [16] and is closely related to that of Eq. (1). The polarization diagram of Fig. 1(g) can be shown [16] to reduce to

$$V_{\rm pol}(r)=-\frac{\alpha_d}{2r^4}, \quad r>1. \tag{4}$$

For $Cl^-$, the dipole polarizability, $\alpha_d$, is the polarizability of the neutral chlorine atom. Kutzner *et al.* [17] used MBPT to determine the frequency-dependent dipole polarizability of chlorine obtaining a static polarizability of 14.8 a.u. (2.19 $Å^3$) in close agreement with a previous calculation by Reinsch and Meyer [18]. The expression in Eq. (4) breaks down at small $r$ but it is customary to modify Eq. (4) to read [16]

$$V_{\rm pol}(r)=-\frac{\alpha_d}{2(r^2+h^2)^2}, \tag{5}$$

where $h$ is on the same scale as the atomic radius but must be determined either phenomenologically or as in the present study by requiring that $V_{\rm pol}(0)$ be approximately equivalent to the energy correction of the valence $3p$ electrons. This condition may be expressed as

$$V_{\rm pol}(0)\approx\Delta E_{\rm SCF}(3p)-|\varepsilon_{3p}|, \tag{6}$$

where $\varepsilon_{3p}$ is the Dirac-Hartree-Fock (DHF) eigenvalue and $\Delta E_{\rm SCF}$ is the absolute value of the difference between the total ground-state self-consistent-field energies of the $Cl^-$ ion and neutral Cl. Reference [16] suggests the use of $1s$ electron energies in Eq. (6). In this work, we are using $3p$ energies since the relatively small excitation energy of the $3p$ electrons causes them to contribute most strongly to the polarizability of the atom. This is equivalent to recognizing that the polarization diagram of Fig. 1(g) is largest when the virtually excited hole state $q$ is a $3p$ orbital. Equations (5) and (6) may be combined to determine the value of the parameter $h$ yielding

$$h=\sqrt[4]{-\alpha_d/\{2[\Delta E_{\rm SCF}(3p)-|\varepsilon_{3p}|]\}} \tag{7}$$

without the need for semiempirical fits. For the negative chloride ion, the energy correction of Eq. (6) was determined using the Oxford multiconfiguration Dirac-Fock computer code of Grant *et al.* [19] to be $\Delta E_{\rm SCF}(3p)-|\varepsilon_{3p}| = -0.055\,249$ a.u., which, combined with $\alpha_d=14.8$ a.u. (2.19 $Å^3$) [17], yields a value $h=3.40$ a.u. for the characteristic cutoff radius. The polarization potential of Eq. (5) is plotted in Fig. 2 along with the expression $-\alpha_d/2r^4$. The electron radial probability density for $Cl^-$ is also plotted to show that the cutoff radius, $h$, has its greatest effect on the potential when the photoelectron is in the vicinity of the atom. The use of the polarization potential of Eq. (5) accounts for polarization in the final state only. The MBPT diagram of Fig. 1(f) corresponding to polarization in the ground state (equivalent to the use of Brueckner orbitals) is not included in any approximate sense in this calculation.

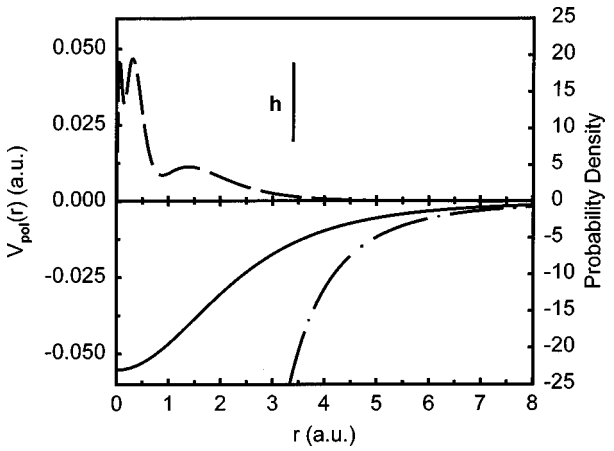


FIG. 2. The solid line represents the polarization potential used in the RRPARP calculations for the negative halide ion $Cl^-$. The dot-dashed line represents the potential $-\alpha_d/2r^4$. The dashed line is the radial probability density for electrons normalized to have an area of 18, the total number of electrons. The characteristic cutoff radius is indicated as $h$.

Photodetachment transition matrix elements were calculated using the RRPA code of Johnson *et al.* [10], the RRPAR, which is a modified RRPA including relaxation effects [11], and the RRPARP, which includes relaxation effects as well as the polarization potential of Eq. (5) added to the single-particle potential for the calculation of RRPA excited-state orbitals. All calculations included interchannel coupling between all 16 dipole-allowed channels in *jj* coupling, namely,

$$1s_{1/2}\rightarrow\varepsilon p_{3/2},\varepsilon p_{1/2},$$

$$2s_{1/2}\rightarrow\varepsilon p_{3/2},\varepsilon p_{1/2},$$

$$2p_{3/2}\rightarrow\varepsilon d_{5/2},\varepsilon d_{3/2},\varepsilon s_{1/2},$$

$$2p_{1/2}\rightarrow\varepsilon d_{3/2},\varepsilon s_{1/2},$$

$$3s_{1/2}\rightarrow\varepsilon p_{3/2},\varepsilon p_{1/2},$$

$$3p_{3/2}\rightarrow\varepsilon d_{5/2}\varepsilon d_{3/2},\varepsilon s_{1/2},$$

$$3p_{1/2}\rightarrow\varepsilon d_{3/2},\varepsilon s_{1/2}.$$

Traditionally, the Dirac-Hartree-Fock eigenvalue energies are used as thresholds for the RRPA [10]. To facilitate comparisons with the experiment of Mandl [2], the calculations used experimental thresholds [20] of 0.1329 and 0.1370 $\pm 10^{-4}$ a.u. for $3p_{3/2}$ and $3p_{1/2}$ electrons, respectively. These

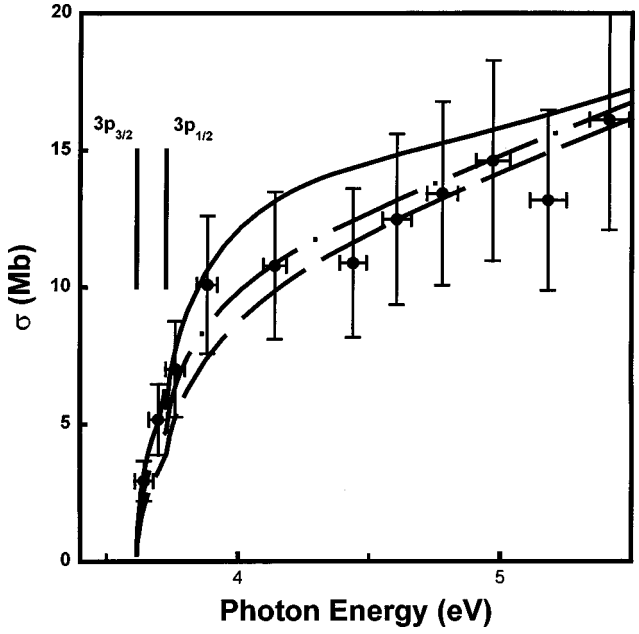


FIG. 3. Photodetachment cross sections above the valence threshold for $Cl^-$. The solid line is RRPA; the dashed line is the RRPAR, which includes relaxation effects; the dot-dashed line is the RRPARP, which includes relaxation and polarization effects. The experimental measurements are from Ref. [2].

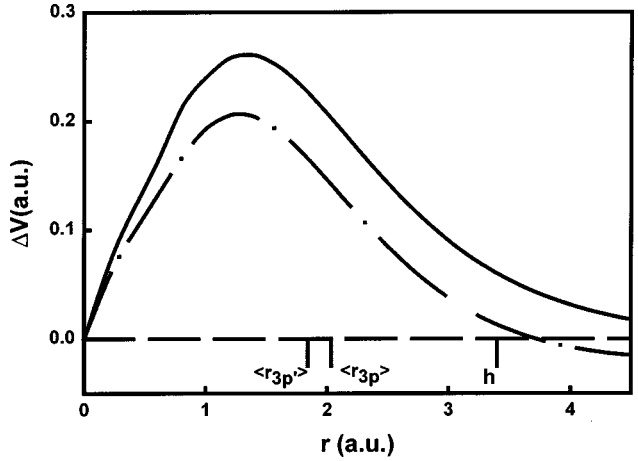


FIG. 4. Difference between direct portions of photoelectron potentials for photodetachment of $Cl^-$. Solid line (dot-dashed line) represents the RRPAR (RRPARP) potential minus the RRPA, frozen-core, potential. The lines indicated by $h$, $\langle r_{3p}\rangle$, and $\langle r_{3p'}\rangle$ represent the cutoff radius for the polarization potential and expectation values of the $3p$ electron radii for the $Cl^-$ ion and the neutral Cl atom, respectively.

energies are consistent with the very accurately measured value of 0.132 764 a.u. reported by Trainham *et al.* [21] for the valence threshold.

The photodetachment cross sections for $Cl^-$ are shown in Fig. 3. Geometric means of length and velocity forms are shown because the geometric mean is less sensitive to the effects of ground-state correlation as demonstrated by Hansen [22]. In the strict RRPA, with Dirac-Hartree-Fock eigenvalue energies used for thresholds and with all channels included, the results are gauge invariant. The present calculations utilize experimental threshold energies [20] which lead to differences in the length and velocity results. The inclusion of relaxation and polarization effects tended to improve the length-velocity agreement in this case. We found that length and velocity cross sections agreed to within 3.12 Mb in the RRPA, 1.55 Mb in the RRPAR, and 0.900 Mb in the RRPARP over the range of energies shown in Fig. 3. The RRPA result is nearly identical to results reported by Radojević *et al.* [8] except that the calculations of Ref. [8] included only seven coupled channels all from the $n=3$ shell. The effects of core relaxation were approximately included using the RRPAR, which calculates the excited-state orbitals in the potential of a relaxed core of electronic orbitals. For the calculation, the hole was placed in the $3p_{3/2}$ subshell since it has the lower threshold and the greatest occupation number. The inclusion of relaxation effectively displaces oscillator strength from near threshold to higher energies, leading to a lower slope for the cross section near threshold. The inclusion of polarization effects increases the slope of the cross section near threshold and increases the value of the cross section at all energies shown.

Earlier in the paper, it was noted that the polarization diagram of Fig. 1(g) tends to cancel the relaxation diagrams of Figs. 1(d) and 1(e) because of the change in sign. Including the polarization potential of Eq. (5) rather than explicitly evaluating the MBPT diagram also has the effect of partially canceling the relaxation effects very close to threshold. In Fig. 4, the variations in the direct parts of the photoelectron potential from the frozen-core potential are shown for the relaxed-core potential as well as for the relaxed-core-with-polarization potential. Core relaxation makes the potential slightly less attractive than the frozen-core potential because the hole is more diffuse. The addition of the polarization potential to the relaxed-core potential reduces the relaxation effect for $r<h$, approximately cancels the effects of relaxation in the vicinity of $r\approx h$, and leads to a slightly more attractive potential for $r>h$.

Although the cutoff radius of the polarization potential, $h$, is determined without the use of parametric fits or reference to experimental data as discussed above, it is important to note the degree of sensitivity of the photodetachment cross section to the value of $h$. In Fig. 5, we present a series of calculations carried out over a range of $h$ values from $h=\infty$ (which corresponds to RRPAR) to $h=1.7$ a.u., corresponding to half of the value of 3.40 a.u. used in the RRPARP calculations presented in Fig. 3. Smaller values of $h$ increase the importance of the polarization potential and raise the value of the cross section. Fortunately, even though the cross section is sensitive to the value of $h$, Eq. (7) indicates that $h$ varies slowly with either the polarizability, $\alpha_d$, or the difference between the DHF and $\Delta E_{\mathrm{SCF}}$ energies.

The branching ratios, $\gamma=\sigma(3p_{3/2})/\sigma(3p_{1/2})$, are shown for the RRPA, RRPAR, and RRPARP in Fig. 6. Spin-orbit splitting causes the branching ratio to be larger than the statistical value of 2 near threshold. Since the RRPA cross sections rise more rapidly at the threshold than the RRPAR and RRPARP, they approach the statistical value at a lower energy.

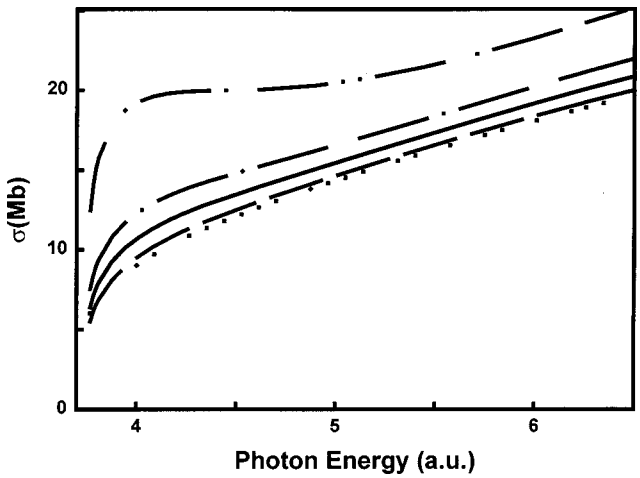


FIG. 5. Photodetachment cross sections for $Cl^-$ above the $3p_{1/2}$ threshold including core-relaxation effects and the polarization potential (RRPARP) with various values of the cutoff radius, *h*. The dotted line represents the RRPAR calculation where no polarization potential is included. The dashed, solid, dot-dashed, and double-dot-dashed lines represent RRPARP calculations where *h* was assigned values 150%, 100%, 75%, and 50% of the value prescribed by Eq. (7).

The angular-distribution asymmetry parameters, $\beta_{3p}$ for the RRPA, RRPAR, and RRPARP, are shown in Fig. 7. The $3p_{3/2}$ and $3p_{1/2}$ $\beta$ parameters have been averaged in the following fashion:

$$\beta_{\mathrm{av}}=\frac{\sigma_{3/2}\beta_{3/2}+\sigma_{1/2}\beta_{1/2}}{\sigma_{3/2}+\sigma_{1/2}} \tag{8}$$

As in the case of the total cross section, the inclusion of relaxation and polarization effects causes substantial changes in the dipole matrix elements, which leads to a notably different prediction for $\beta_{3p}$. It is important to note the contrast between $\beta_{3p}$ for $Cl^-$ and for neutral argon [23] due to the very different nature of the potential for outgoing photoelectrons.

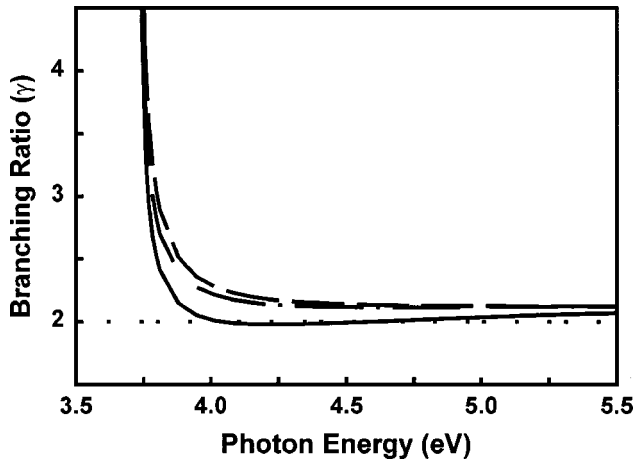


FIG. 6. Branching ratio, $\gamma=\sigma(3p_{3/2})/\sigma(3p_{1/2})$, for $Cl^-$. Solid line is RRPA, dashed line is RRPAR, and dot-dashed line is RRPARP. The statistical value of 2 is indicated by the dotted line.

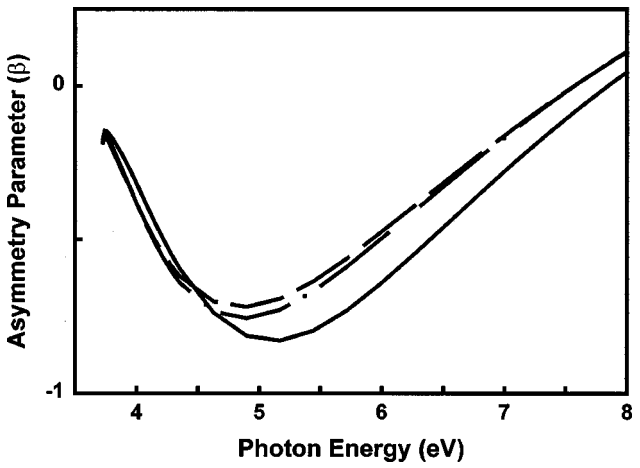


FIG. 7. Angular-distribution asymmetry parameter, $\beta_{3p}$, for threshold photodetachment of $Cl^-$. Solid line is RRPA, dashed line is RRPAR, and dot-dashed line is RRPARP.

The inverse process of photodetachment is radiative attachment of an electron to the neutral atom. This process may be interesting in the case of rarefied systems as in astrophysical conditions. The principle of detailed balancing relates the radiative attachment cross section to the photodetachment cross section in the following way [1]:

$$\sigma_{\mathrm{att}}(\omega)=\frac{g_{\mathrm{ion}}}{g_{\mathrm{atom}}}\frac{k^2}{q^2}\sigma_{\mathrm{det}}(\omega), \tag{9}$$

where $g_{\mathrm{ion}}$ and $g_{\mathrm{atom}}$ are the statistical weights for the ion and atom, respectively, $k=\omega/c$ is the photon wave number, and $q$ is the wave number of the electron given by

$$q=\sqrt{2(\omega-I)} \tag{10}$$

in atomic units, with $I$ being the threshold energy.

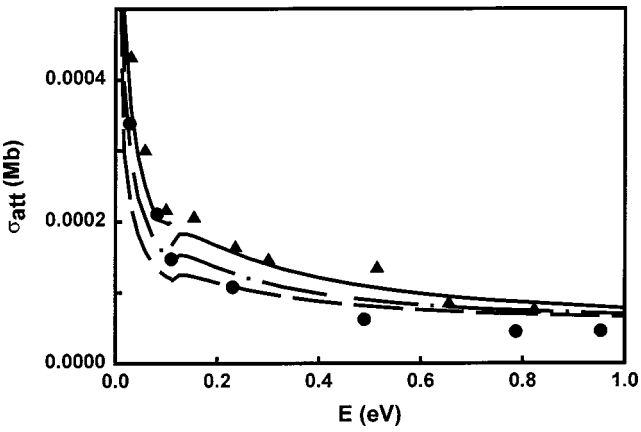


FIG. 8. Radiative attachment cross sections for the neutral chlorine atom. The solid line is RRPA, the dashed line is RRPAR, and the dot-dashed line is RRPARP. The experimental data indicated by solid triangles are derived from the photodetachment cross section of Ref. [2]. Solid circles are experimental measurements of Ref. [1].

The radiative attachment cross sections for the RRPA, RRPAR, and RRPARP were calculated using Eq. (9) with the partial $3p_{3/2}$ partial cross sections with $g_{\mathrm{ion}}=1$ and $g_{\mathrm{atom}}=4$. The results are presented in Fig. 8. We have also applied Eq. (9) to the experimental total photodetachment cross section of Mandl [2], which we show along with the experimental radiative attachment cross sections [1]. For experimental data with energy below the $3p_{1/2}$ threshold, we used the $3p_{3/2}$ experimental threshold energy [20] and $g_{\mathrm{atom}}=4$; for data above the $3p_{1/2}$ threshold we used an average experimental energy weighted by the occupation numbers of the two subshells and $g_{\mathrm{atom}}=6$. Since the Wigner threshold law predicts a photodetachment cross section which varies as $q^{2l+1}$ near threshold, by Eq. (9) the radiative attachment cross sections follow a $q^{-1}$ relationship for the capture of $s$ electrons near threshold.

In conclusion, three models have been employed to calculate the photodetachment and radiative attachment cross sections of $Cl^-$, the RRPA, the RRPAR (which includes relaxation effects), and the RRPARP (which includes relaxation and polarization effects). Polarization effects are found to partially cancel relaxation effects and improve agreement with experiment [2]. Precise experimental measurements are desirable and would aid in testing the accuracy of the *ab initio* polarization potential used here. To further evaluate the generality of the model, it should be applied to more species of negative ions and neutral atoms. It would be interesting, for example, to compare the $4d$ subshell photoionization cross sections for barium and xenon calculated using the polarization potential of Eq. (5) with previous calculations using MBPT relaxation and polarization diagrams [12].

## ACKNOWLEDGMENTS

The authors wish to thank V. Radojević for use of the RRPAR code and Walter Johnson for use of the RRPA code. We thank Stephen Vance of Brookhaven National Laboratory for his unique insights into this problem. Discussions with the late Hugh P. Kelly provided the initial motivation for applying the polarization potential to this system. This work has been supported in part by Grant No. PHY-9707183 of the National Science Foundation and by the Office of Scholarly Research of Andrews University.

[1] B. M. Smirnov, in *Negative Ions*, edited by H. S. W. Massey (McGraw-Hill, New York, 1982).
[2] A. Mandl, Phys. Rev. A **14**, 345 (1976).
[3] D. E. Rothe, J. Quant. Spectrosc. Radiat. Transf. **9**, 49 (1969); H.-P. Popp, Phys. Rep. **16**, 169 (1975).
[4] E. J. Robinson and S. Geltman, Phys. Rev. **153**, 4 (1967).
[5] Z. D. Qian and H. P. Kelly (private communication).
[6] T. Ishihara and T. C. Foster, Phys. Rev. A **9**, 2350 (1974).
[7] T. N. Rescigno, C. F. Bender, and V. B. McKoy, Phys. Rev. A **17**, 645 (1978).
[8] V. Radojević, H. P. Kelly, and W. R. Johnson, Phys. Rev. A **35**, 2117 (1987).
[9] M. Kutzner, M. Felton, and D. Winn, Phys. Rev. A **45**, 7761 (1992).
[10] W. R. Johnson and C. D. Lin, Phys. Rev. A **20**, 964 (1979); W. R. Johnson, C. D. Lin, K. T. Cheng, and C. M. Lee, Phys. Scr. **21**, 403 (1980).
[11] V. Radojević, M. Kutzner, and H. P. Kelly, Phys. Rev. A **40**, 727 (1989).
[12] M. Kutzner, Z. Altun, and H. P. Kelly, Phys. Rev. A **41**, 3612 (1990).
[13] C. H. Greene and M. Aymar, Phys. Rev. A **44**, 1773 (1991).
[14] F. Robicheaux and C. H. Greene, Phys. Rev. A **46**, 3821 (1992).
[15] D. W. Norcross, Phys. Rev. Lett. **32**, 192 (1974).
[16] M. Ya. Amusia, in *Atomic Photoeffect*, edited by P. G. Burke and H. Kleinpoppen (Plenum, New York, 1990).
[17] M. Kutzner, H. P. Kelly, D. J. Larson, and Z. Altun, Phys. Rev. A **38**, 5107 (1988).
[18] E. A. Reinsch and W. Meyer, Phys. Rev. A **14**, 915 (1976).
[19] I. P. Grant, B. J. McKenzie, P. H. Norrington, D. F. Mayers, and N. C. Pyper, Comput. Phys. Commun. **21**, 207 (1980).
[20] R. S. Berry *et al.*, J. Chem. Phys. **49**, 127 (1968).
[21] R. Trainham, G. D. Fletcher, and D. J. Larson, J. Phys. B **20**, L777 (1987).
[22] A. E. Hansen, Mol. Phys. **13**, 425 (1967).
[23] M. Kutzner, Q. Shamblin, S. E. Vance, and D. Winn, Phys. Rev. A **55**, 248 (1997).